Transient coherence of media under strong phase modulation exploiting electromagnetically induced transparency

David Shwa and Nadav Katz
Racah Institute of Physics, The Hebrew University, Jerusalem 91904, Israel
(Received 25 December 2013; revised manuscript received 22 June 2014; published 29 August 2014)

When quantum systems are shifted faster than their transition and coupling time scales, their susceptibility is dramatically modified. We measure the optical susceptibility of a strongly modulated electromagnetically induced transparency system. Time vs detuning plots for different pump modulation frequencies reveal a transition between an adiabatic regime where a series of smooth pulses are created and a nonadiabatic regime where a strong transient oscillating response is added. Applying a magnetic field lifts the hyperfine level degeneracy, revealing an interference effect between the different magnetic level transients. We explore the dynamics of the magnetic and nonmagnetic cases and discuss their coherent nature. We finally combine the global phase of the transmitted pulses with the transient interference to achieve broadband magnetic sensing without losing the sensitivity of a single electromagnetically induced transparency line.

DOI: 10.1103/PhysRevA.90.023858 PACS number(s): 42.50.Gy, 07.55.Ge, 32.60.+i, 32.80.Xx

I. INTRODUCTION

Electromagnetically induced transparency (EIT) is a coherent process, where a strong coupling field creates a narrow transmission band in the probe spectrum in an otherwise fully absorptive medium [1,2]. The narrow linewidth of EIT makes it suitable for applications in many fields such as extreme slow light [3], quantum storage devices [4], nonlinear optics [5], and high-sensitivity magnetic sensors [6]. On the other hand, this narrow linewidth directly limits the bandwidth of data that can be processed. A signal which has a broader bandwidth than the EIT linewidth will be filtered such that only part of the pulse having the EIT linewidth will be transmitted and delayed [7,8]. In terms of sensing this means that although a very high sensitivity is possible using EIT, it is a problem to probe with this sensitivity a broadband field in a simple way. Possible solutions to this problem may arise from different approaches. One idea is to use a heterodyne measurement of the EIT signal with a broadband probe [8] using the interference of the dispersive part of the EIT [9]. This may offer an increased resolution and broaden the sensing bandwidth since the dispersive part is decaying in a slower manner. In order to get a more substantial bandwidth another idea is to use a multimode EIT system where each EIT line still has a narrow bandwidth but spreading the signal across many systems allows for a broader signal. Such systems were devised spatially [10] and spectrally [11,12] for larger data capacity as well as for broadband magnetic sensing [13,14]. A different approach is to use dynamic EIT where the transient response may have a much broader bandwidth than steady state EIT. The transient response of an EIT media to a sudden switching [15–18] as well as for an ac magnetic field [19] was explored theoretically and experimentally for various regimes. For a constant detuning the decay of the transients is dictated by the EIT linewidth, while the frequency of the transient oscillations equals the two photon detuning [16,18]. The detuning can be larger than the linewidth leading to an underdamped oscillator response. In the case of a linear sweep through the resonance the frequency of the transient is chirped [18] and behaves similarly to a Landau-Zener (LZ) transition [20,21]. Transients have also been used as a magnetic sensing technique to measure the Earth's magnetic field with $1\frac{nT}{\sqrt{\text{Hz}}}$ sensitivity [22,23].

In this article we take both the concepts of multimode spectrum and transient dynamics and combine them to create a new method for measuring coherent effects. Using a full mapping of the transient response of an EIT system as a function of the detuning we observe the transition from an adiabatic regime to a nonadiabatic regime. We also measure the complex interference pattern that arises when a magnetic field is applied. In this case an interference between transients from three Zeeman sublevels is visible. The problem of three-level crossing in the context of LZ transitions was addressed both theoretically and experimentally [24–28]. Here we have the ability to change the levels' energy gap experimentally implementing the three-level crossing for variable level detuning. Moreover, we show that by using this interference combined with a broadband phase modulation sweep a wideband high-sensitivity magnetometer can be achieved.

II. THEORY

We now describe the effect a phase-modulated strong coupling field has upon the temporal shape of a probe pulse going through an EIT media. The coupling field can be written as follows:

$$\mathbf{E_c}(t) = E_{c0}e^{[i\omega_c t - i\phi(t)]}, \tag{1}$$

where E_{c0} is the amplitude of the coupling field, ω_c is the optical frequency, and $\phi(t)$ is the time-dependent phase modulation. In order to describe the change in the probe field due to this modulated coupling field the full spatiotemporal Maxwell-Bloch equations for an EIT system need to be solved [29]. In the case of long enough interaction media and perturbative probe intensity the system can reach a steady state solution. The EIT susceptibility in this case has only temporal dependence and no spatial dependence. For a susceptibility with no temporal dependence the probe transmission amplitude, $p(t)$, is given by the convolution of the entering signal, $E_p(\omega)$, and the susceptibility, $\chi(\omega)$; hence $p(t) = \mathcal{F}[E_p(\omega)\chi(\omega)]$. In the case of a modulated field

the susceptibility is time dependent, and this convolution is not valid. A possible way of solving this problem is by taking the spectral decomposition of the susceptibility $\chi(\omega,t)=\sum_{n=-\infty}^{\infty}e^{in\Omega t}\chi_n(\omega)$. Now the transmission is just $p(t)=\sum_{n=-\infty}^{\infty}e^{in\Omega t}\mathcal{F}[E_p(\omega)\chi_n(\omega)]$ [29]. We use a sinusoidal modulation; hence $\phi(t)=M\sin(\Omega_c t)$, where M is the modulation depth and $\Omega_c=2\pi f_c$ is the modulation frequency. The spectrum of such a modulated field can be described as a sum of Bessel functions:

$$e^{-i\phi}=\sum_{n=-\infty}^{\infty}e^{in\Omega_c t}J_n(-M). \tag{2}$$

The spectrum of this modulation has narrow peaks separated by the frequency Ω_c. The Bessel functions' amplitude drops sharply for $n\gg M$, thus creating a full modulation span of $2M\Omega_c$. The transfer function in this case is just an infinite comb of single EIT lines [1] weighted by Bessel functions:

$$\chi(t)=\sum_{n=-\infty}^{\infty}i\alpha\frac{J_n(-M)e^{in\Omega_c t}}{\Gamma-i(\Delta-n\Omega_c)+\frac{R_c^2}{\gamma_{12}-i(\delta-n\Omega_c)}}. \tag{3}$$

Here $\alpha=\frac{N\mu^2}{\epsilon_0\hbar}$ is the two-level absorption coefficient, with N being the density of the atoms and μ being the transition dipole moment; Γ is the homogeneous decay rate; γ_{12} is the decoherence rate of the two ground states; $R_c=\frac{\mu E_{c0}}{\hbar}$ is the Rabi frequency of the coupling field which is phase modulated; Δ is the one-photon detuning of the probe field; and δ is the two-photon detuning.

In the case of the D1 line of warm ^{87}Rb vapor with buffer gas the full width at half maximum EIT linewidth is [30] $\gamma_{\rm EIT}=2(\gamma_{12}+\frac{R_c^2}{\Gamma_D+\Gamma})$, where Γ_D is the Doppler broadening. This linewidth is usually a few kHz, which is much narrower than the pressure-broadened homogeneous linewidth ($\Gamma\sim$ 100 MHz) and the Doppler broadening ($\Gamma_D\sim 500$ MHz); thus the probe two level susceptibility is effectively constant for the full modulation bandwidth as long as $M\Omega_c\ll\Gamma$.

Applying a magnetic field removes the Zeeman degeneracy and the energy levels of the hyperfine levels will create a ladder according to the Zeeman splitting of the two lower levels with the Larmor frequency $\mu_B B(g_F m_F-g_{F'}m_{F'})$. B here is the magnetic field, μ_B is the Bohr magneton, and g_F is the Landé coefficient of the hyperfine level. We can write the transfer function in this case as follows:

$$\chi(t)=\sum_{n=-\infty}^{\infty}\sum_{m_F=-F}^{F}\sum_{m_{F'}=-F'}^{F'}i\alpha \times\frac{J_n(-M)e^{in\Omega_c t}}{\Gamma-i(\Delta-n\Omega_c)+\frac{R_c^2}{\gamma_{12}-i[\delta-n\Omega_c-\mu_B B(g_F m_F-g_{F'}m_{F'})]}}. \tag{4}$$

The EIT susceptibility is similar to that of Eq. (3) with the exception of a splitting to several EIT peaks having a certain phase between them according to the Zeeman frequency splitting.

III. EXPERIMENTAL SETUP

The experimental setup is shown in Fig. 1. For an EIT Λ scheme we use the hyperfine transitions of the D1 line of

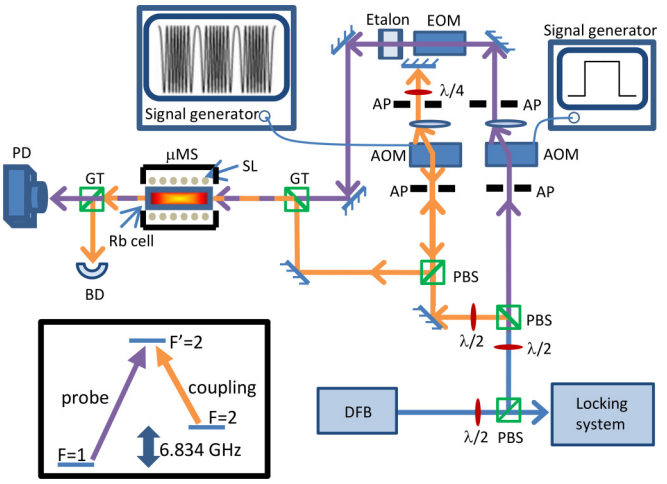

FIG. 1. (Color online) The experimental setup. DFB, distributed feedback laser; PBS, polarizing beam splitter; AP, aperture; AOM, acousto-optic modulator; EOM, electro-optic modulator; GT, Glan-Taylor polarizer; μMS, μ-metal shield; BD, beam dump; PD, photodiode; SL, solenoid.

^{87}Rb. A DFB laser locked to the $F=2\rightarrow F'=2$ transition is split into probe and coupling beams using a polarizing beam splitter. The phase modulation over the coupling field as well as the pulse creation of the probe is done using acousto-optic modulators. In order to bring the probe to resonance with the $F=1\rightarrow F'=2$ transition an electro-optic modulator is used. The beams (orthogonal polarization) are combined using a Glan-Taylor polarizer and pass through a 7.5-cm cell containing an isotopically pure ^{87}Rb (>95%) with 10 Torr Ne as the buffer gas heated to ~40 °C. The cell is shielded against an outside magnetic field using three layers of μ metal. An axial magnetic field is created using a uniform solenoid. After the cell another polarizer is used in order to filter the coupling field while the probe is detected using an amplified photodiode.

IV. RESULTS

Figure 2 demonstrates the transmission temporal response of a square probe pulse with an intensity of 0.05 mW/cm^2

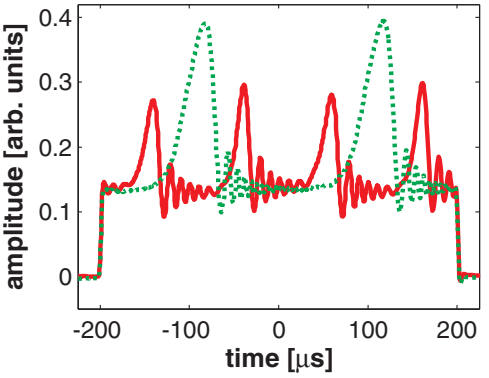

FIG. 2. (Color online) Transient oscillations of the probe amplitude due to coupling modulation with $f_c=5$ kHz and $M=20$. Red line, $\delta=0$; green dotted line, $\delta=100$ kHz.

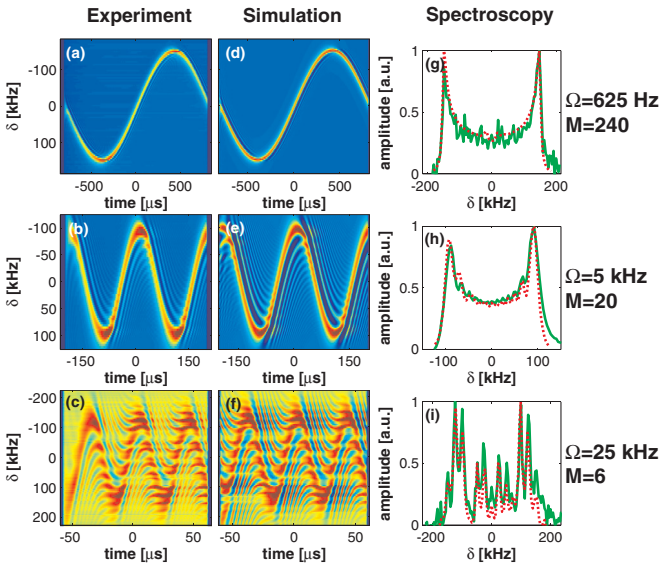

FIG. 3. (Color online) Adiabatic to nonadiabatic transition. 2D mapping of the spectrotemporal response of the probe pulse is demonstrated in the case of (a) the adiabatic regime, (b) the intermediate regime, and (c) the nonadiabatic regime. The parameters of the modulation are (a) $f_c = 625$ Hz and $M = 240$, (b) $f_c = 5$ kHz and $M = 20$, and (c) $f_c = 25$ kHz and $M = 6$. All the experiments are done with $\gamma_{\rm EIT} = 14$ kHz. Plots (d)–(f) show a simulation of the three regimes that takes into account Eq. (3) with the parameters written above. Plots (g)–(i) show the spectrum of the transmission taken as the time integral for each frequency. Green line, experimental spectrum; red dotted line, simulation spectrum.

due to a phase-modulated coupling field with an intensity of 1 mW/cm^2 in an EIT media. Two major features are observed. One is a train of pulses that is created with a period and phase that is dependent upon the coupling-field modulation frequency and the detuning [29]. The second feature is a transient ringing that is associated with the response of the media to a sudden change in the susceptibility. This ringing has a chirped frequency as expected [18]. It decays with a characteristic time that depends upon $1/\gamma_{\rm EIT}$ and the chirp rate through the transition (see Sec. V for more details). The instantaneous frequency of the coupling field due to the modulation is $\omega(t) = \omega_c + \frac{\partial \phi}{\partial t} = \omega_c + M\Omega_c \cos(\Omega_c t)$ while the response has the spectral width of the EIT linewidth; thus the relation between the modulation frequency and the EIT width sets the adiabaticity of the response.

Figure 3 shows experimentally and theoretically the transition between the adiabatic regime where the modulation frequency is lower than the EIT linewidth ($\Omega_c \ll \gamma_{\rm EIT}$) and the nonadiabatic regime where $\Omega_c \gg \gamma_{\rm EIT}$. For both regimes the phase of the pulses is determined by the instantaneous frequency hence we see a sinelike plot as a function of the detuning with a period $1/\Omega_c$ and an amplitude $M\Omega_c$. In the adiabatic regime the transients decay fast enough so they are hardly noticeable, but as the modulation frequency becomes comparable to the EIT linewidth [Fig. 3(b)] the transient ringing is clearly observed. In the nonadiabatic regime the modulation frequency is faster than the decay of the transient ringing, creating an interference between consecutive pulses as can be observed in Fig. 3(c). Simulation of these two-dimensional (2D) patterns using Eq. (3) are depicted in Figs. 3(c)–3(e), showing a striking similarity to the results. One aspect this linear response theoretical simulation fails to take into account is the smearing of the interference pattern when the probe pulse is turned on as can be visualized particularly in Fig. 3(c). The cause of this effect is the gradual buildup of the dark-state polariton and consequently the creation of the EIT line that has a characteristic time of $1/2\pi\gamma_{\rm EIT}$ [16]. Integrating the time domain reveals the steady state spectrum of the probe light. Figures 3(f)–3(h) show the integrated spectra of the experimental data (green line) as well as the simulation (red line) in the adiabatic and nonadiabatic regimes. These spectra fit to the phase modulation spectrum according to the Fourier expansion of Eq. (2), meaning a δ function separated by the modulation frequency, broadened due to the finite EIT linewidth.

Figure 4 shows a 2D mapping of the temporal response of the probe for different magnetic fields (The two-photon detuning is on resonance with the magnetic-insensitive transition).

In the adiabatic regime [Fig. 4(a)] it is possible to see a splitting of the sole pulse in $B = 0$ into three pulses. These pulses correspond to three EIT lines that are present in the spectrum. For the D1 line of rubidium, using an arbitrary magnetic field, up to seven EIT lines may appear [31]. Due to the vectorial nature of the magnetic interaction, the relative strength of these lines depends on the angle between the beam direction and the magnetic field as well as on the polarization of the pump and probe beams [6]. The specific configuration we use in our setup is $\mathbf{B} \parallel \mathbf{k}$ with linear polarization. In this case only three lines appear in the spectrum [6,32]. As a complementary measurement we also measure the steady state

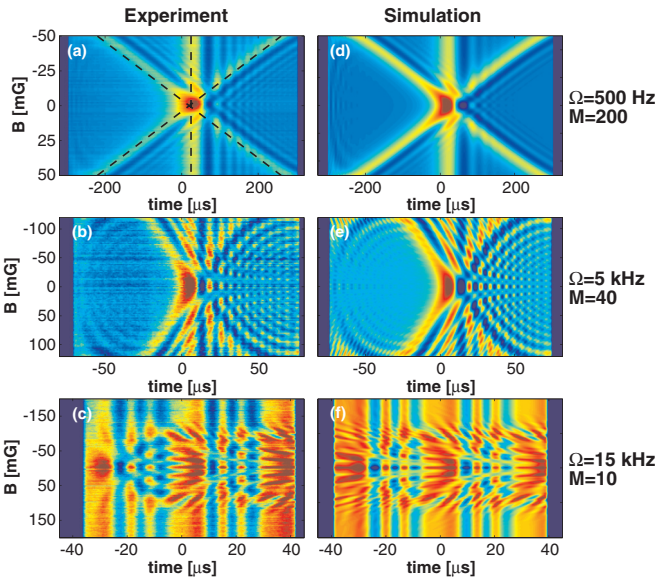

FIG. 4. (Color online) Temporal response of a probe pulse due to the magnetic field for (a) the adiabatic regime, (b) the intermediate regime, and (c) the nonadiabatic regime. The parameters of the modulation are (a) $f_c = 500$ Hz and $M = 200$, (b) $f_c = 5$ kHz and $M = 40$, and (c) $f_c = 15$ kHz and $M = 10$. Plots (d)–(f) show a simulation of the three regimes that takes into account Eq. (4) with the parameters written above.

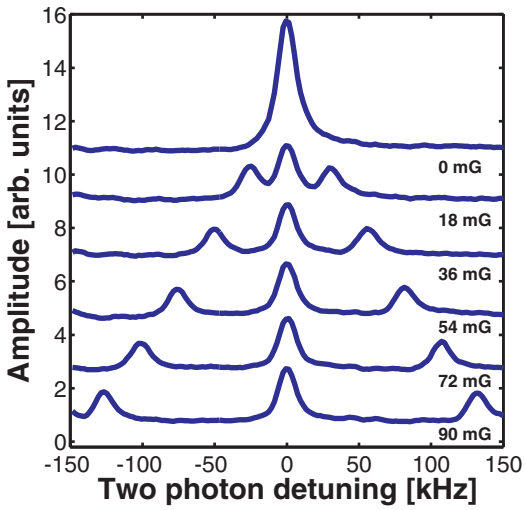

FIG. 5. (Color online) Zeeman splitting of EIT resonance due to axial magnetic field. The spectrums are shifted for clarity. The observed spectrum is indeed split to three levels.

spectrum of the EIT under variable magnetic field as can be seen in Fig. 5.

To understand better the behavior of the three pulses a broad scan of the probe transmission vs the magnetic field is shown in Fig. 6. We can distinguish clearly the functional behavior of the three EIT lines for $\Delta m = 0, \pm 2$. The $\Delta m = 0$ line is not dependent upon the magnetic field; thus its phase is constant with a pulse every half-cycle. Both $\Delta m = \pm 2$ lines are sinusoidally modulated with a cycle equal to f_c and a phase of π between them. Each of these two lines behave exactly like the detuning sweep of one EIT line (with no magnetic field) under phase modulation (see, for example, Fig. 3). This feature is understandable, as applying the magnetic field can be translated to detuning via the Larmor frequency Zeeman shift.

Figures 4(b) and 4(c) show the nonadiabatic regime where every pulse has an oscillating tail with a certain phase causing an interference pattern. This interference can be used for broadband magnetic sensing as described in Sec. VI. A simulation based on Eq. (4) is shown in Figs. 4(d)–4(f), having the same basic features as the experimental results.

Adding a constant detuning creates a symmetric shift of the two sinusoids until reaching a field larger than $2M\Omega$ (results not shown). In this case the two sinusoids get separated

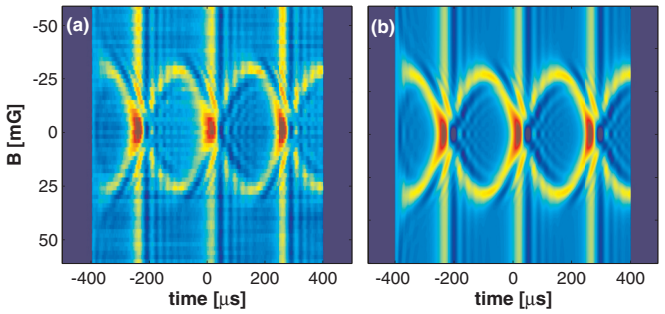

FIG. 6. (Color online) A broad scan both in time and in magnetic field sweep. Here $f_c = 2$ kHz and $M = 10$. (a) Experiment. (b) Simulation.

and the constant pulse of $\Delta m = 0$ disappears. Since the two sinusoids do not intersect the interference pattern disappears. The major consequence is that measuring a constant magnetic field accurately using this method is possible only for magnetic fields with Larmor frequency smaller than $2M\Omega$.

The observed interference may be understood in the following way. In the case of hyperfine EIT in a buffer gas and under the condition of $\gamma_{\mathrm{EIT}} \ll \Gamma$ it is possible to treat the two ground states as a degenerate set of effective two-level systems (TLSs) [33,34]. Adding a magnetic field removes the degeneracy and splits each TLS according to the Zeeman frequency [35]. In our case due to the selection rules stated above the splitting is to three groups with $\Delta m = 0, \pm 2$. As a consequence of this picture it is possible to think of the magnetic sweep in time as a chirp of the three TLSs [as depicted by the black dashed lines in Fig. 4(a)]. Thus, the interference we measure is a direct consequence of a three-level degeneracy. It is important to notice that in EIT, due to the strong coupling field, the population remains in the dark state all the time and the measured interference is not a three-level LZ population transition but rather a coherence measurement. A more intuitive way of describing the LZ dynamics in our system is presented in the following section.

V. DRESSED STATES REPRESENTATION

The ringing observed in Fig. 2 is a manifestation of a nonadiabatic transition through the EIT resonance. LZ theory deals with this kind of transition and gives an analytic prediction to the population transfer between the levels. In the case of an EIT in buffer gas the best way to describe the system is using the dressed states picture. Taking the Hamiltonian of the bare three levels under the rotating wave approximation

$$\begin{pmatrix} 0 & 0 & \frac{1}{2}R_p^* \\ 0 & \delta & \frac{1}{2}R_c^*(t) \\ \frac{1}{2}R_p & \frac{1}{2}R_c(t) & \Delta \end{pmatrix}, \tag{5}$$

where $R_c(t) = R_{c0}e^{-i\phi(t)}$, R_p are the Rabi frequencies of the coupling and the probe fields, respectively, δ is a constant two-photon detuning, and Δ is the one-photon detuning which in the case relevant to us is 0. In order to elucidate the resemblance to the LZ model it is instructive to change to a new basis where

$$\begin{aligned} |1\rangle' &= |1\rangle, \\ |2\rangle' &= |2\rangle e^{-i\phi(t)}, \\ |3\rangle' &= |3\rangle e^{i\phi(t)}. \end{aligned} \tag{6}$$

The new Hamiltonian becomes

$$\begin{pmatrix} 0 & 0 & \frac{1}{2}R_p^* \\ 0 & \delta - \frac{1}{2}\frac{\partial\phi}{\partial t} & \frac{1}{2}R_{c0}^* \\ \frac{1}{2}R_p & \frac{1}{2}R_{c0} & \frac{1}{2}\frac{\partial\phi}{\partial t} \end{pmatrix}. \tag{7}$$

The 2×2 matrix of levels $|2'\rangle$ and $|3'\rangle$ is a LZ Hamiltonian. Under EIT conditions $R_c \gg R_p$; hence it is possible to diagonalize this 2×2 matrix with two new dressed levels with eigenvalues $\epsilon_{\pm} = -\frac{1}{2}\delta \pm \frac{1}{2}\sqrt{\delta^2 + R_{c0}^2 + (\frac{\partial\phi}{\partial t})^2 - 2\frac{\partial\phi}{\partial t}\delta}$. In the simple case where $\delta = 0$ these states are just $|+\rangle = \sin\theta|2'\rangle + \cos\theta|3'\rangle$ and $|-\rangle = \cos\theta|2'\rangle - \sin\theta|3'\rangle$

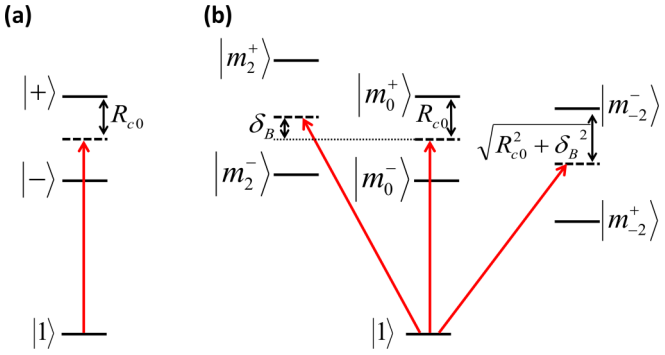

FIG. 7. (Color online) Dressed states [on two-photon resonance ($\delta = 0$)] for (a) no magnetic field and (b) with magnetic field. Red arrows represent probe transition on resonance.

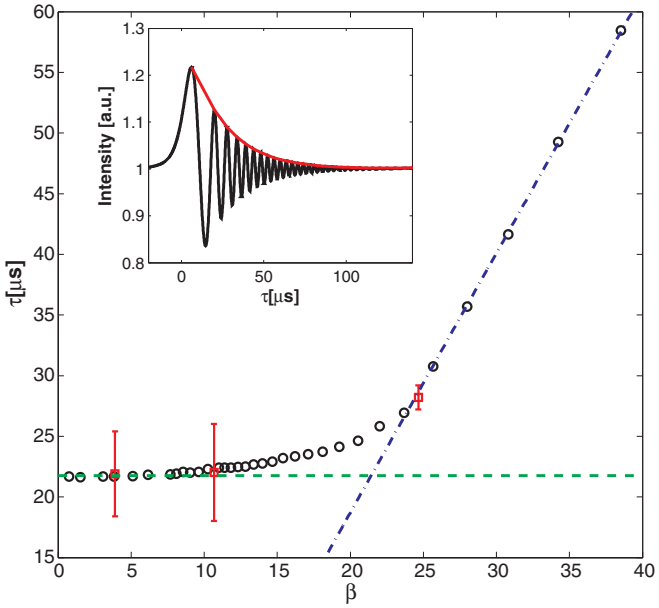

FIG. 8. (Color online) Decay time of the probe ringing as a function of β. Black circles, simulation; red squares, experiment. The decay time is calculated using an exponential fit to the peaks of the ringing as shown in the inset. Green dashed line, the EIT decay according to $2/2\pi\gamma_{\rm EIT}$; blue dash dotted line, linear fit for the adiabatic case. Simulation parameters are similar to the ones in Fig. 3 with variable modulation index and modulation frequency.

with $\tan 2\theta = {}^{R_{c0}}/_{\frac{\partial\phi}{\partial t}}$ [36]. It is important to notice that no actual population is being transferred between the two levels since only level $|1\rangle$ is populated at all times. This two-dressed-state dynamics is interrogated by the probe field, meaning that the transition matrix element $|1\rangle \rightarrow |3\rangle$ we are measuring in the experiment carries the dynamics described above as depicted in Fig. 7(a). In our experiment a phase modulation sweep in time causes a periodic crossing between the two dressed levels.

When a magnetic field is applied the system is split into three subsystems with three levels in each [35]. Each one of these subsystems behaves exactly as a single EIT system with a magnetic Zeeman shift, $\delta_B = \mu_B B(g_F m_F - g_{F'} m_{F'})$. As a consequence the energy levels of the subsystems $\Delta m = +2$ and $\Delta m = -2$ are reversed with respect to the magnetic field (with $\delta = 0$) while the energy levels of the subsystems $\Delta m = 0$ are only shifted by the pump field as depicted in Fig. 7(b).

One interesting characterization of the LZ dynamics is the transition time. This time can be measured by the relaxation time of the oscillations after the transition [37]. The two parameters that determine the transition's properties are the coupling Rabi frequency and the chirp rate, defined as $\partial^2\phi/\partial t^2$. In the case of a sinusoidal phase modulation, where $\phi(t) = M\cos(\Omega t)$, the maximal chirp rate for $\delta = 0$ is $\partial^2\phi/\partial t^2 = M\Omega^2$. It is useful to quantify the transition using the dimensionless parameter $\beta = \frac{R_c}{\sqrt{\partial^2\phi/\partial t^2}} = \frac{R_c}{\sqrt{M\Omega}}$. Figure 8 shows the relaxation time, τ, as a function of β for our experimental results (red squares) as well as for our simulation results (black circles). The relaxation time is found from an exponential fit to the ringing peaks as depicted in the inset in Fig. 8. The probability of a LZ transition (without decoherence) with respect to time is a parabolic cylinder function that can be approximated in the case of the relaxation time to a chirped oscillatory function multiplied by some polynomial decay [37]. Adding decoherence will add an exponential decay to the LZ relaxation. Our fit is indeed not to the full function, but to an exponential decay, which allows a qualitative estimation for the LZ relaxation as a function of β. We see that in the diabatic limit (low β) the decay time is nearly constant and converging towards $2/2\pi\gamma_{\rm EIT}$, meaning LZ relaxation which is much longer than decoherence relaxation. At the adiabatic limit (high β) the decay is linear with β. Similar theoretical results for the LZ theory have been reported before [37,38], but with different scaling of β.

VI. MAGNETIC SENSING

The dynamic pattern created by the phase modulation as depicted in Fig. 4 can be used for broadband magnetic sensing. Each magnetic field has a certain characteristic pulse timing associated with it. The phase of the first pulse is a prominent feature for broad magnetic sensing as the total amplitude of the modulation is $B_{\rm max} = M\Omega/\Delta m\mu_B g_F$. This corresponds to 142 and 107 mG for Figs. 4(b) and 4(c), respectively. Moreover, the interference pattern offers a way of measuring accurately the magnetic field in the area of the interference. The sensitivity to the magnetic field is dependent upon the signal (S) to noise ($\widetilde{N}$) ratio and is given by [13]

$$\frac{\Delta B}{\sqrt{\Delta\nu}} = \frac{\sqrt{t}}{S/\widetilde{N}} = \frac{\sqrt{t}\widetilde{N}}{\partial A/\partial B}, \tag{8}$$

where t is the measurement time and $\partial A/\partial B$ is the gradient of the integrated measured amplitude and the magnetic field. In our case, since the transient ringing is a complex multifrequency feature the best way to characterize the transients for different magnetic fields is by using the correlation between them. Using this method we measured the noise and the gradient of the correlation function and estimated our sensitivity to be 1 nT/$\sqrt{\rm Hz}$ for the 5 kHz modulation and 0.2 nT/$\sqrt{\rm Hz}$ in the case of 15 kHz. This sensitivity is similar to the one reported by Belfi *et al.* using a modulated coherent population trapping system [13]. The ultimate sensitivity for a given sensing system

is [39] $\frac{\delta B}{\sqrt{\text{Hz}}} = \frac{\hbar}{\mu_B g_F}\sqrt{\frac{2\pi\gamma_{\text{EIT}}}{NV}}$, where V is the volume of the magnetometer. In our case this sensitivity is $\sim$400 fT/$\sqrt{\text{Hz}}$, well below the observed sensitivity. Better shielding and electronics are expected to approach this limit. A different way of evaluating the sensitivity of our method is by analyzing the interferogram created by the multilevel interference as can be seen, for example, in Fig. 4(b). Simulation shows that the width of the central peaks (around $B = 0$) narrows linearly as the number of Zeeman levels participating in the interference grows, meaning higher interferometric sensitivity. A similar effect of multi Zeeman sublevel interference was measured in cold atoms yielding a corresponding enhancement in the sensitivity [40].

VII. CONCLUSIONS

We present a method for measuring broadband coherent effects using the transient dynamics of a strongly modulated system. Specifically, we show the transient response of an EIT media to a phase-modulated pump. This response reveals explicitly the coherent nature of the EIT susceptibility. In the nonadiabatic regime where EIT peaks are spectrally resolved we clearly observe interference between the different modes. Albeit the interference between these modes does not contribute to EIT spectral narrowing and as a consequence to a slower light propagation [12,41], it does create a transient behavior useful for broadband data transfer. Applying a magnetic field splits the EIT line into three, allowing us to see an interference pattern dynamics. Along with the wideband sweep due to the high modulation index it is shown to be a useful tool for sensitive wideband magnetometry.

ACKNOWLEDGMENTS

We acknowledge helpful discussions with N. Davidson, M. Kiffner, and T. Dey and support of the Bikura (ISF) under Grant No. 1567/12.

[1] M. Fleischhauer, A. Imamoglu, and J. P. Marangos, Rev. Mod. Phys. **77**, 633 (2005).
[2] I. Novikova, R. L. Walsworth, and Y. Xiao, Laser Photonics Rev. **6**, 333 (2012).
[3] L. V. Hau, S. E. Harris, Z. Dutton, and C. H. Behroozi, Nature (London) **397**, 594 (1999).
[4] L.-M. Duan, M. D. Lukin, J. Cirac, and P. Zoller, Nature (London) **414**, 413 (2001).
[5] M. Jain, H. Xia, G. Y. Yin, A. J. Merriam, and S. E. Harris, Phys. Rev. Lett. **77**, 4326 (1996).
[6] V. I. Yudin, A. V. Taichenachev, Y. O. Dudin, V. L. Velichansky, A. S. Zibrov, and S. A. Zibrov, Phys. Rev. A **82**, 033807 (2010).
[7] J. Tidström, P. Jänes, and L. M. Andersson, Phys. Rev. A **75**, 053803 (2007).
[8] R. N. Shakhmuratov and J. Odeurs, Phys. Rev. A **71**, 013819 (2005).
[9] M. D. Lukin, M. Fleischhauer, A. S. Zibrov, H. G. Robinson, V. L. Velichansky, L. Hollberg, and M. O. Scully, Phys. Rev. Lett. **79**, 2959 (1997).
[10] Z. Dutton, M. Bashkansky, M. Steiner, and J. Reintjes, Opt. Express **14**, 4978 (2006).
[11] D. D. Yavuz, Phys. Rev. A **75**, 031801 (2007).
[12] G. Campbell, A. Ordog, and A. I. Lvovsky, New J. Phys. **11**, 103021 (2009).
[13] J. Belfi, G. Bevilacqua, V. Biancalana, Y. Dancheva, and L. Moi, J. Opt. Soc. Am. B **24**, 1482 (2007).
[14] Y. V. Vladimirova, V. N. Zadkov, A. V. Akimov, A. Y. Samokotin, A. V. Sokolov, V. N. Sorokin, and N. N. Kolachevsky, Appl. Phys. B: Lasers Opt. **97**, 35 (2009).
[15] A. D. Greentree, T. B. Smith, S. R. de Echaniz, A. V. Durrant, J. P. Marangos, D. M. Segal, and J. A. Vaccaro, Phys. Rev. A **65**, 053802 (2002).
[16] F. Meinert, C. Basler, A. Lambrecht, S. Welte, and H. Helm, Phys. Rev. A **85**, 013820 (2012).
[17] Y. Q. Li and M. Xiao, Opt. Lett. **20**, 1489 (1995).
[18] S. J. Park, H. Cho, T. Y. Kwon, and H. S. Lee, Phys. Rev. A **69**, 023806 (2004).
[19] L. Margalit, M. Rosenbluh, and A. D. Wilson-Gordon, Phys. Rev. A **85**, 063809 (2012).
[20] W. Harshawardhan and G. S. Agarwal, Phys. Rev. A **55**, 2165 (1997).
[21] M. B. Kenmoe, S. C. Kenfack, A. J. Fotue, A. B. Tchapda, M. Tchoffo, L. C. Fai, J. E. Danga, M. E. Ateuafack, and M. P. Djemmo, arXiv:1307.3878.
[22] L. Lenci, S. Barreiro, P. Valente, H. Failache, and A. Lezama, J. Phys. B: At. Mol. Opt. Phys. **45**, 215401 (2012).
[23] L. Lenci, A. Auyuanet, S. Barreiro, P. Valente, A. Lezama, and H. Failache, Phys. Rev. A **89**, 043836 (2014).
[24] C. E. Carroll and F. T. Hioe, J. Phys. A: Math. Gen. **19**, 1151 (1986).
[25] B. M. Garraway and N. V. Vitanov, Phys. Rev. A **55**, 4418 (1997).
[26] L. Gaudreau, G. Granger, A. Kam, G. C. Aers, S. A. Studenikin, P. Zawadzki, M. Pioro-Ladrière, Z. R. Wasilewski, and A. S. Sachrajda, Nat. Phys. **8**, 54 (2011).
[27] S. S. Ivanov and N. V. Vitanov, Phys. Rev. A **77**, 023406 (2008).
[28] J. Lin and N. A. Sinitsyn, J. Phys. A: Math. Theor. **47**, 015301 (2014).
[29] M. Kiffner and T. N. Dey, Phys. Rev. A **79**, 023829 (2009).
[30] E. Figueroa, F. Vewinger, J. Appel, and A. I. Lvovsky, Opt. Lett. **31**, 2625 (2006).
[31] K. Cox, V. I. Yudin, A. V. Taichenachev, I. Novikova, and E. E. Mikhailov, Phys. Rev. A **83**, 015801 (2011).
[32] S. A. Zibrov, I. Novikova, D. F. Phillips, R. L. Walsworth, A. S. Zibrov, V. L. Velichansky, A. V. Taichenachev, and V. I. Yudin, Phys. Rev. A **81**, 013833 (2010).
[33] N. V. Vitanov and S. Stenholm, Phys. Rev. A **55**, 648 (1997).
[34] Y. Wu, Phys. Rev. A **54**, 1586 (1996).
[35] A. V. Tavǐchenachev, V. I. Yudin, R. Wynands, M. Stähler, J. Kitching, and L. Hollberg, Phys. Rev. A **67**, 033810 (2003).

[36] D. A. Steck, *Quantum and Atom Optics*, available online at http://steck.us/teaching (Revision 0.8.3, 25 May 2012).
[37] N. V. Vitanov, Phys. Rev. A **59**, 988 (1999).
[38] K. Mullen, E. Ben-Jacob, Y. Gefen, and Z. Schuss, Phys. Rev. Lett. **62**, 2543 (1989).
[39] D. Budker and M. Romalis, Nat. Phys. **3**, 227 (2007).
[40] J. Petrovic, I. Herrera, P. Lombardi, F. Schäfer, and F. S. Cataliotti, New J. Phys. **15**, 043002 (2013).
[41] S. E. Harris, Phys. Rev. Lett. **70**, 552 (1993).